[30] Wallace, J.M., Eckelmann, H. and Brodkey, R.S., The wall region in turbulent shear flow, *J. Fluid Mech.*, 54(1), 39–48, 1972.
[31] Walsh, M.J., Turbulent boundary layer drag reduction using riblets, *AIAA Paper* 82–0169, 1982.
[32] Willmarth, W.W. and Lu, S.S., Structure of the Reynolds stress near the wall, *J. Fluid Mech.*, 55(1), 65–92, 1972.

13.5 Wall-Bounded Turbulent Flows

David G. Bogard and Karen A. Thole

Introduction

For wall-bounded turbulent flows, the very high shear near the wall leads to instabilities that ultimately are the source of much of the turbulence production. These flows can be classified as either external flows (boundary layers) or internal flows (pipes or ducts). The turbulence generated near the wall results in bulk movement of fluid to and from the wall region. This causes a very large increase in transport of momentum resulting in considerably larger wall shear than would occur with a laminar flow. For practical engineering design purposes, prediction of wall shear for turbulent wall flows is generally of prime importance. Empirical correlations based on relevant geometrical and boundary layer parameters to predict the wall shear for many generic turbulent wall flows are presented in this section. In some cases, for more complex flows the wall shear may be predicted computationally with turbulence models of various degrees of sophistication (computational modeling for turbulent flows is discussed in Chapter 14).

As described in Section 13.1, turbulence consists of eddies with a wide range of sizes. The scale of the largest turbulent eddies for wall-bounded flows is dictated by the width of the turbulent shear layer (this is similar to free shear layers). For a boundary layer this is the boundary layer thickness, δ, and for internal flows this is the pipe radius, R, or channel half-height, $h/2$. However, for wall-bounded flows the wall imposes a further limit to the scale of turbulent eddies — eddies close to the wall are constrained to be a size of the order of the distance from the wall, y. Consequently, wall-bounded turbulent shear layers have two distinct length scales. Near the wall the effect of the wall manifests itself through viscous effects (except for rough walls) and the turbulent structure scales with the viscous length scale ν/u_τ. The wall friction velocity, $u_\tau = \sqrt{\tau_w/\rho}$, is the characteristic velocity scale for the turbulent fluctuating velocities. Consequently, wall-bounded flows have two distinct regions: an inner region where the viscous scaling (ν/u_τ) dominates, and an outer region where scaling with respect to the shear layer width dominates. These are often referred to as inner scaling and outer scaling, respectively. The inner region typically extends to about 0.15 δ, and is similar for all (smooth) wall-bounded flows. The outer region characteristics are dependent on the type of wall-bounded flow, i.e., internal or external flows, and on external conditions such as pressure gradients and free-stream turbulence levels.

This section describes the characteristics of turbulent wall flows in terms of mean velocity profiles and the statistics of the turbulent fluctuating velocities. These characteristics of turbulent wall flows are discussed for fundamental (canonical) flows, i.e., two-dimensional with smooth and flat walls; and for more complex (noncanonical) flows involving external influences or different wall characteristics.

Turbulent Shear Stress

Before proceeding with discussions of specific turbulent wall flows, it is informative to describe the nature of the increased momentum transport for a turbulent wall flow. The fundamental mechanics responsible for increased momentum transport are shown by the following analysis of the Reynolds-Averaged Navier–Stokes equation (the RANS equation presented in Section 13.1). For wall-bounded turbulent flows with thin shear layers, this equation can be simplified considerably. The following equations

are obtained based on conditions of two-dimensional mean flow, i.e., the mean velocity and all gradients in the z direction are negligible. For external flows the RANS equation can be simplified by assuming negligible gradients in the streamwise direction, because generally the width of the shear layer is much smaller than the streamwise extent of the flow. Therefore the following approximations are valid (often referred to as the boundary layer assumptions):

$$\begin{aligned} \overline{U} &>> \overline{V} \\ \overline{W} &= 0 \\ \frac{\partial}{\partial y} &>> \frac{\partial}{\partial x}, \frac{\partial}{\partial z} = 0 \end{aligned} \tag{13.44}$$

Neglecting insignificant terms based on the above approximations, the x and y components of the RANS equation become

$$\rho\overline{U}\frac{\partial\overline{U}}{\partial x} + \rho\overline{V}\frac{\partial\overline{U}}{\partial y} = -\frac{\partial\overline{P}}{\partial x} + \frac{\partial}{\partial y}\left(\mu\frac{\partial\overline{U}}{\partial y} - \rho\overline{u'v'}\right) \tag{13.45}$$

$$0 = -\frac{1}{\rho}\frac{\partial\overline{P}}{\partial y} - \frac{\partial\overline{v'^2}}{\partial y} \tag{13.46}$$

For fully developed internal flows the V velocity component and streamwise gradients of all velocity components are zero, so the x-momentum equation reduces to

$$0 = -\frac{d\overline{P}}{dx} + \frac{\partial}{\partial y}\left(\mu\frac{\partial\overline{U}}{\partial y} - \rho\overline{u'v'}\right) \tag{13.47}$$

Note that the equations for x-momentum are similar to the equations that would be obtained for a laminar flow except for the additional turbulent shear stress term $-\rho\overline{u'v'}$. As discussed in Section 13.1, the turbulent shear stress terms are really apparent stresses due to convective transport by the turbulent eddies. The total shear stress is comprised of the sum of the viscous stress, $\tau_{vis} = \mu\partial\overline{U}/\partial y$, and the turbulent shear stress $\tau_{turb} = -\rho\overline{u'v'}$. The dominance of the turbulent stresses across most of the shear layer is evident in Fig. 13.19. Very close to the wall, turbulent shear stress becomes negligible and the viscous term dominates. This occurs because the scale of turbulent fluctuations near the wall reduce to a small enough level so that they are strongly damped by the fluid viscosity. Within a very short distance ($y^+ > 10$), however, turbulent shear stress becomes dominant. Note that the total stress, $\tau_{total} = \tau_{vis} + \tau_{turb}$, is approximately constant, and equal to the wall shear stress, for a short distance away from the wall. This region of constant total stress (it actually decreases slowly with distance from the wall) is known as the "constant stress" layer.

Canonical Flows: Pipes, Channels, and Boundary Layers

Whether or not a wall bounded flow is turbulent largely depends on the Reynolds number. Turbulent flow generally occurs in a pipe for Reynolds numbers of $\mathrm{Re}_D > 2,300$, and in a two-dimensional duct for Reynolds numbers of $\mathrm{Re}_h > 3000$. For an aerodynamically smooth flat plate, the boundary layer is initially laminar, passes through a transition phase, and becomes turbulent at point which ranges between $\mathrm{Re}_x = 10^5$ to 3×10^6. Except for controlled laboratory conditions, the precise Reynolds number for which the flow will become turbulent is generally not predictable because of sensitivity to initial conditions and external disturbances. Furthermore, for pipe or duct flows, a development distance downstream of the entrance is required before the turbulence is fully developed. At a point approximately $x/D = 20$ to 40 downstream of the entrance for pipe flow, or $x/h = 20$ to 100 for channel flow, mean velocity profiles become fully developed (invariant with streamwise distance). However, the distance required to achieve fully developed profiles for the turbulent fluctuating velocity statistics is several times longer.

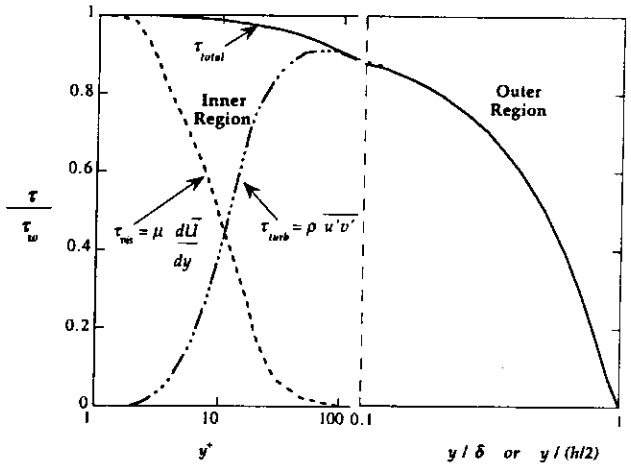

FIGURE 13.19 Turbulent and viscous shear stress levels across boundary layer and channel flows.

Wall Shear Correlations

For many engineering calculations, wall shear for a turbulent wall flow is generally determined from empirical correlations. By convention, for pipe flows the wall shear is expressed in terms of the nondimensional friction factor f, and for channel flows and boundary layers wall shear is typically expressed in terms of the skin friction coefficient, C_f. Correlations for f and C_f for a range of Reynolds numbers are presented in Table 13.1. The correlation for f for pipe flows is based on a fit to the Prandtl's universal law of friction [21] which has been verified by the extensive experiments of Nikuradse [20] up to $\mathrm{Re}_D = 3.4 \times 10^6$. The correlation of C_f for two-dimensional channel flow was recommended by Dean [8] based on a review of a wide range of experimental studies. Dean also recommends a minimum aspect ratio (width/height) of 7:1 to ensure two-dimensional flow at the center of the channel.

Determining wall shear for an external boundary layer flow is inherently more complex than for an internal flow, because the wall shear varies with distance along the surface. One of the Cf correlations for a flat plate, external boundary layer presented in Table 13.1 is in terms of the Reynolds number based on distance $x(\mathrm{Re}_x)$ where x is the length of surface over which the flow has traveled. This correlation seems most convenient since Re_x is easily calculated. However, this ease of application is misleading, since the correlation was developed based on an assumption of a turbulent boundary layer from the start of the surface. In fact, typically the boundary layer flow will initially be laminar for some distance, followed by a distance of transitional flow, and finally become fully turbulent farther downstream. Although correlations exist that account for different lengths of laminar and turbulent boundary layer flows [26], these require knowledge of the effective point of transition, which can vary from $\mathrm{Re}_x = 10^5$ to 3×10^6, and is typically difficult to predict.

The second C_f correlation for turbulent boundary layer flows in Table 13.1 is in terms of Reynolds number based on the momentum thickness $\theta(\mathrm{Re}_\theta)$. The momentum thickness is a measure of the momentum deficit at a given position in the boundary layer and is defined in terms of an integration across the boundary layer profile as follows:

$$\theta = \int_0^\infty \frac{\rho \overline{U}}{\rho_\infty \overline{U}_\infty} \left(1 - \frac{\overline{U}}{\overline{U}_\infty}\right) dy \tag{13.48}$$

The ratio of momentum thickness to boundary layer thickness varies slightly with Reynolds number, but is typically $\theta/\delta \approx 0.1$ where δ is the boundary layer thickness defined as the point at which the mean velocity is $0.99\overline{U}_\infty$. Accurate determination of θ requires measurements very close to the wall. However, because θ is based on an integral across the boundary layer profile, it is generally more precise than δ.

TABLE 13.1 Skin Friction Correlations

Geometry	Correlation	Comments
Flat plate $C_f = \frac{\tau_w}{\frac{1}{2}\rho U_\infty^2}$	$C_f = \frac{0.455}{\ln^2(0.06\ \mathrm{Re}_x)}$	White [25] $4 \times 10^5 < \mathrm{Re}_x < 10^{10}$
Flat plate	$C_f = 0.036\ \mathrm{Re}_\theta^{-0.3}$	$\mathrm{Re}_\theta < 3000$
	$C_f = 0.014\ \mathrm{Re}_\theta^{-0.18}$	$\mathrm{Re}_\theta > 3000$
Rough surface flat plate, fully-rough flow	$C_f = \left(1.4 + 3.7 \log \frac{x}{k}\right)^{-2}$	White [25] $x/k > 100$
Channel flow $C_f = \frac{\tau_w}{\frac{1}{2}\rho U_m^2}$	$C_f = 0.073\ \mathrm{Re}_h^{-0.25}$	Dean [8] $6 \times 10^3 < \mathrm{Re}_h < 6 \times 10^5$
Pipe flow $f = \frac{8\tau_w}{\rho U^2}$	$f = \frac{0.25}{\left\{\log\left[\frac{\epsilon/D}{3.7} + \frac{2.51}{\mathrm{Re}\sqrt{f}}\right]\right\}^2}$	Colebrook [6] Gerhart, et al. [10] $4 \times 10^3 < \mathrm{Re}_D < 10^7$

The correlations for C_f in terms of Re_θ are curve fits based on the C_f distribution tabulated by Coles [7]. These correlations based on Re_θ are more reliable than that based on Re_x because they are independent of the upstream development of the boundary layer.

For experimental investigations, a turbulent boundary layer is often induced to occur by using a "trip" device. Trips that have commonly been used include a short length of sand paper and small diameter cylinders. For these flows, a virtual origin can be defined as the point upstream where the boundary layer would have started in order to obtain the same downstream boundary layer thickness without use of a trip. Given a measurement of the momentum thickness θ at some position following the trip, the distance to the virtual origin of the turbulent boundary layer can be established by matching the C_f correlation equation based on Re_θ with that based on Re_x.

Mean Velocity Profiles

The mean velocity profiles over a range of Reynolds numbers for both boundary layer and channel flows are shown in Fig. 13.20a. The wall normal distance, y, has been nondimensionalized accordingly with either the boundary layer thickness δ or the channel half-height $h/2$. Note that the boundary layer mean velocity profiles have similar profiles for a wide range of Reynolds numbers, but there is a slight shift to larger $\overline{U}/\overline{U}_\infty$ as Re^* increases ($\mathrm{Re}^* = \delta u_\tau/\nu$ or $(h/2)u_\tau/\nu$). Better scaling for the outer region of the boundary layer is obtained using the defect velocity scaled with u_τ, i.e., $(\overline{U} - \overline{U}_\infty)/u_\tau$. Also, the Clauser thickness Δ is often used rather than δ since it can be determined more precisely. The Clauser thickness is defined as

$$\Delta = \int_0^\infty \frac{\overline{U}_\infty - \overline{U}}{u_\tau} dy \tag{13.49}$$

The slightly larger values for $(\overline{U}/\overline{U}_\infty)$ for the channel flow in Fig. 13.20a are due to fundamental differences in the outer regions for these two classes of flows (to be discussed later).

The same mean velocity profiles presented in Fig. 13.20a are presented in Fig. 13.20b in which the near wall region has been emphasized by using a log scale for y/δ. The failure of the outer scaling to collapse the profiles in the near wall region is clear in Fig. 13.20b. Near the wall the mean velocity profiles scale with the inner variables: friction velocity, u_τ, and viscous length scale, ν/u_τ. Inner scaling results in nondimensional velocities $u^+ = \overline{U}/u_\tau$ and wall normal distance $y^+ = yu_\tau/\nu$, and the resulting mean velocity profiles for external and internal flows are shown in Fig. 13.20c and 13.20d, respectively. With

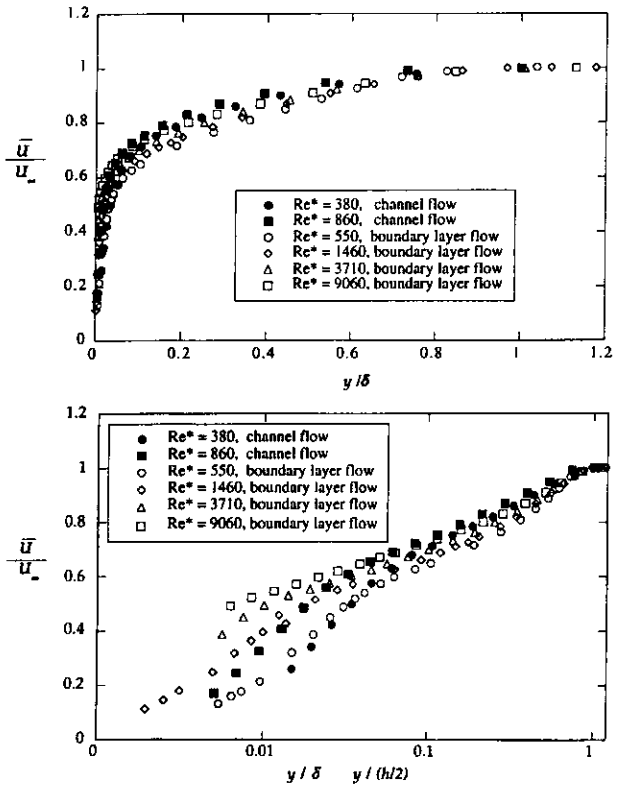

FIGURE 13.20 Mean velocity profiles for boundary layer and channel flows; $Re^* = 380$ and 860 from Harder and Tiederman [12], $Re^* = 550$ and 1460 from Koske and Tiederman [17], and $Re^* = 3710$ and 9060 from Bruns et al. [3]. (a) Outer scaling, (b) expanded outer scaling,

this inner scaling, the mean velocity profile near the wall is invariant with Reynolds number and is similar for all wall flows, internal and external. The inner region of the boundary layer extends from the wall to nominally $y/\delta \approx 0.15$. The inner region can be further subdivided into three distinct regions — the viscous sublayer, buffer layer, and the log-law region — as shown in Fig. 13.20c and 13.20d.

The region very close to the wall is known as the viscous sublayer and is between $0 < y^+ < 5$. Here the viscous shear is dominant and the turbulent shear stress is negligible, resulting in the following relation for the mean velocity profile:

$$u^+ = y^+ \tag{13.50}$$

Between y^+ 30 and $y/\delta \approx 0.15$, the mean velocity is logarithmic in nature, hence the term log-law region. In this region, the velocity is represented by

$$u^+ = \frac{1}{k} \ln y^+ + C \tag{13.51}$$

where κ, known as the Von Kármán constant, and C are empirically determined constants. The values of the constants used in Fig. 13.20c are $\kappa = 0.41$ and $C = 5.0$ as recommended by Coles [7]. The log-law region corresponds to a region were the inner and outer scaling overlap, i.e., the velocity profile simultaneously scales with both inner and outer parameters. Matching the inner and outer scaling of the mean velocity profile leads to an analytical prediction of the log-linear velocity profile.

The buffer layer represents an intermediate layer between the viscous sublayer and the log-law region. The following single equation representing the mean velocity profile from the wall through the log-law

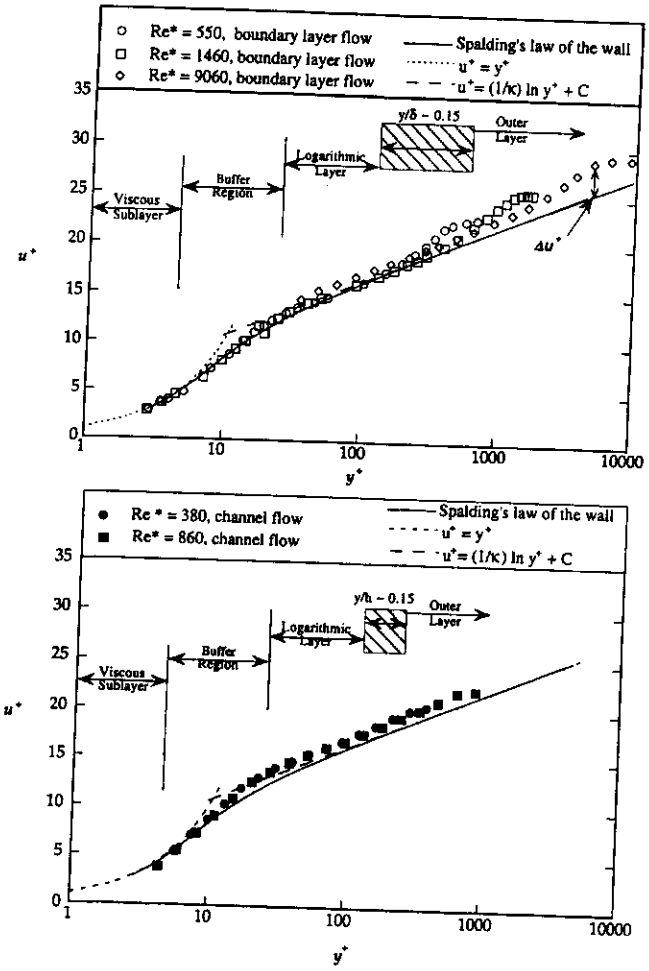

FIGURE 13.20 Mean velocity profiles for boundary layer and channel flows; $Re^* = 380$ and 860 from Harder and Tiederman [12], $Re^* = 550$ and 1460 from Koske and Tiederman [17], and $Re^* = 3710$ and 9060 from Bruns et al. [3]. (a) Outer scaling, (b) expanded outer scaling, (c) inner scaling.

region was suggested by Spalding [23]:

$$y^+ = u^+ + e^{-\kappa C}\left[e^{\kappa u^+} - 1 - \kappa u^+ - \frac{(\kappa u^+)^2}{2} - \frac{(\kappa u^+)^3}{6}\right] \tag{13.52}$$

In the outer part of the boundary layer, the profiles shown in Fig. 13.20c show a distinct increase in u^+ relative to an extrapolation of the log-law curve. This outer part of the velocity profile is known as the wake region. The deviation of the velocity profile from the log-law is generally quantified in terms of the wake strength Π which is defined as

$$\Pi = \frac{\kappa\left(\Delta u^+\right)}{2} \tag{13.53}$$

where Δu^+ is the maximum deviation of the mean velocity from the log-law profile as shown on Fig. 13.20c. An equation for the mean velocity profile including the wake region is obtained by using a wake function

$W(y/\delta) \approx 2\sin^2(\frac{\pi}{2}\frac{y}{\delta})$ as follows:

$$u^+ = \frac{1}{\kappa}\ln y^+ + C + \frac{\Pi}{\kappa}W\left(\frac{y}{\delta}\right) \tag{13.54}$$

For boundary layer flows the wake strength is zero at very low Reynolds numbers, increasing to a constant value of $\Pi = 0.55$ for $\mathrm{Re}_\theta > 5,000$. Note that the wake strength for the channel flow is much smaller than for the boundary layer flow. This difference in wake strength can be attributed to the intermittency of the turbulence in the outer region. For the outer region of turbulent wall flows, external flows are significantly different from internal flows in that only external flows have a region of intermittent turbulence. Intermittency, γ, is defined at a point in the flow as the fraction of time the flow is turbulent at that point, i.e., $\gamma = 1$ would indicate continuous turbulence. Internal flows are continuously turbulent, but for external flows, nonturbulent free-stream fluid is intermingled with turbulent eddies in the outer part of the boundary layer. Typically, for a zero pressure gradient boundary layer flow, the flow is continuously turbulent, $\gamma = 1.0$, from the wall to a distance $y/\delta = 0.6$ from the wall. Beyond $y/\delta = 0.6$ the intermittency decreases falling to levels of $\gamma = 0.5$ by $y/\delta = 0.9$, and $\gamma = 0.2$ at the edge of the boundary layer.

Turbulent Fluctuations and Shear Stresses

Knowledge of the characteristics of turbulent fluctuations and shear stresses in turbulent wall flows is based primarily on experimental measurements. Although direct numerical simulations have recently added to this data base, these simulations are limited to low Reynolds numbers. Before discussing these characteristics, a cautionary word about the accuracy of the experimental measurements is in order. Practically all measurements of these turbulence statistics have been made with either hot-wire anemometry systems or laser Doppler velocimeters. For hot-wire anemometry, inaccuracies occur when the length of the sensor is greater than the smallest turbulence length scale. This is particularly a problem for measurements close to the wall and at higher Reynolds numbers. Several studies have been conducted to establish maximum sensor lengths and spacing for accurate measurements, including Johansson and Alfredsson [14], Nakayama and Westphal [19], and Browne et al. [2]. Much of the data presented in this section were measured with laser Doppler velocimeters (LDV) which have good spatial resolution, but can have signal processing concerns [9].

Profiles of the turbulent velocity fluctuations u'_{rms}, v'_{rms}, and w'_{rms} for boundary layer and channel flows are presented in Fig. 13.21a and 13.21b; and profiles for turbulent shear stress $\overline{u'v'}$ and the correlation coefficient $R_{uv} = \overline{u'v'}/u'_{rms} \cdot v'_{rms}$ are presented in Fig. 13.21c. Note that the velocity fluctuations in Fig. 13.21 are nondimensionalized with u_τ, which is the appropriate scaling velocity across the boundary layer or internal flow. The distributions of u'_{rms} shown in Fig. 13.21a, which cover a wide range of Reynolds numbers for boundary layers and also include channel flows, show the collapse of the profiles near the wall ($y^+ < 30$) using y^+, with a distinct peak of $u'_{rms}/u_\tau \approx 2.8$ at $y^+ = 15$. Away from the wall the profiles do not collapse with this inner scaling, but do collapse with outer scaling for $y/\delta > 0.15$ (not shown). At the highest Reynolds number shown in Fig. 13.21a the u'_{rms} profile shows a second peak somewhat further from the wall, but still within the near wall region. Note that the rate of decay of u'_{rms} in the outer part of the boundary layer is somewhat greater than that for the channel flow, which may be attributed to the difference in the intermittency discussed previously. Also, the minimum u'_{rms} levels in the outer region for the channel flow data shown in Fig. 13.21a represent the centerline values.

Near the wall there are large differences in the levels of the u'_{rms}, v'_{rms}, and w'_{rms} turbulent fluctuations as is evident in Fig. 13.21b. Wall normal fluctuations are most directly suppressed by the wall resulting in lower values of v'_{rms} relative to the other components. Both v'_{rms} and w'_{rms} have maximum levels over broad regions in the log-law region rather than the sharp peak near the wall as for u'_{rms}. In the outer region, the u'_{rms}, v'_{rms}, and w'_{rms} levels converge. Although there are some indications of increasing levels of v'_{rms} and w'_{rms} with increasing Reynolds numbers, the near wall distributions shown in Fig. 13.21b are

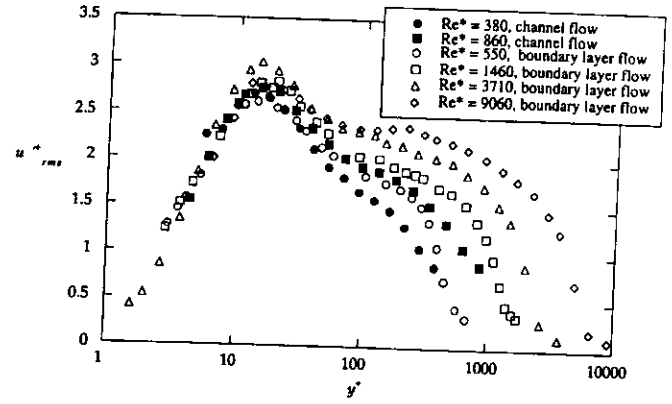

(a)

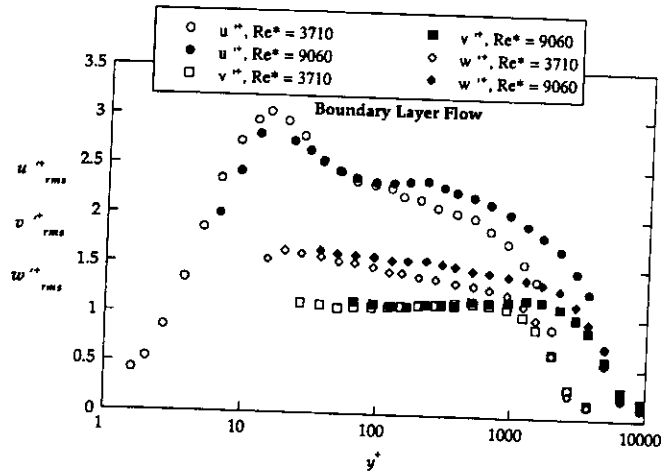

(b)

FIGURE 13.21 RMS velocity fluctuations and Reynolds shear stresses for boundary layer and channel flows; $Re^* = 380$ and 860 from Harder and Tiederman [12], $Re^* = 550$ and 1460 from Koske and Tiederman [17], and $Re^* = 3710$ and 9060 from Bruns et al. [3]. (a) u'_{rms} for a range of Re^*, (b) comparison of u'_{rms} v'_{rms} w'_{rms}

relatively Reynolds number independent. The distributions of u'_{rms}, v'_{rms}, and w'_{rms} in the outer region are Reynolds number independent when scaled with y/Δ.

Recall that the Reynolds shear stress is the turbulence contribution to the total stress. Consequently, when the Reynolds shear stress is normalized with the wall shear stress, $\overline{u'v'}/u_\tau^2$, the maximum magnitude is 1.0. Profiles of $\overline{u'v'}/u_\tau^2$ presented in Fig. 13.21c show that Reynolds shear stress approaches this maximum in the log-law region and then decreases in the outer region due to streamwise pressure gradients for internal flows, or due to boundary layer growth for external flows. The range of different curves in the outer region collapses to a single curve when scaled with y/Δ. In the viscous sublayer, $\overline{u'v'}/u_\tau^2$ decreases to essentially zero. Also shown in Fig. 13.21c is the profile for the correlation coefficient R_{uv}. For internal and external flows there is a very broad region with a constant value of $R_{uv} \approx -0.4$ that is independent of Reynolds number.

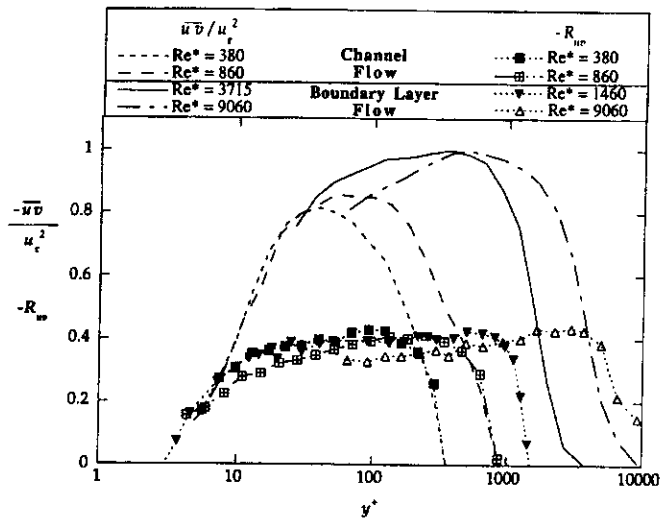

(c)

FIGURE 13.21 (c) $\overline{u'v'}$ and R_{uv} for a range of Re*.

Energy Spectra and Length Scales

The power spectral density measured at a point in a turbulent flow gives an indication of the turbulence energy content at different frequencies. Physically, the measured velocity oscillations are essentially due to the size of eddies convecting through the measurement point, so the frequency of a measured turbulent fluctuation is more appropriately interpreted in terms of the inverse of the size the turbulent eddy, i.e., the wavenumber $\boldsymbol{k}$. The frequency f (in Hz) of a measured quantity can be converted to wavenumber k_1 using $k_1 = 2\pi f/\overline{U}$. Note that in general the wavenumber $\boldsymbol{k}$ is a vector quantity, and k_1 is the wavenumber component in the direction of flow. A typical power spectrum for wall bounded turbulent flows in shown in Fig. 13.22a, where $E_{11}(k_1)$ is the power spectral density for the u' fluctuating velocity component. The measured power spectra in Fig. 13.22a are compared to a theoretical equation for isotropic turbulence with no viscous dissipation developed by Von Kármán [13] which is as follows:

$$\frac{2\pi E_{11}(k_1)}{\overline{u'^2_{rms}}\Lambda_x} \frac{4}{\left\{1+\left[4\Lambda_x k_{1/3}\right]^2\right\}^{5/6}} \tag{13.55}$$

where Λ_x is the streamwise integral length scale defined as

$$\Lambda_x = \int R_{11}(r)dr \tag{13.56}$$

and the autocorrelation R_{11} is defined as

$$R_{11} = \frac{\overline{u(x)\cdot u(x+r)}}{u'^2_{rms}} \tag{13.57}$$

where r is a displacement distance in the x-direction. The integral length scale is a measure of the largest scale of the turbulent eddies and is typically $\Lambda_x \approx 0.4\delta$ across much of the boundary layer.

Equation (13.56) can be reformulated in terms of the limiting value of the power spectrum as k_1 approaches zero, yielding the following equation for the integral length scale Λ_x:

$$\Lambda_x = \frac{E_{11}(k_1)_{k_1\to 0}}{4u'^2_{rms}} \tag{13.58}$$

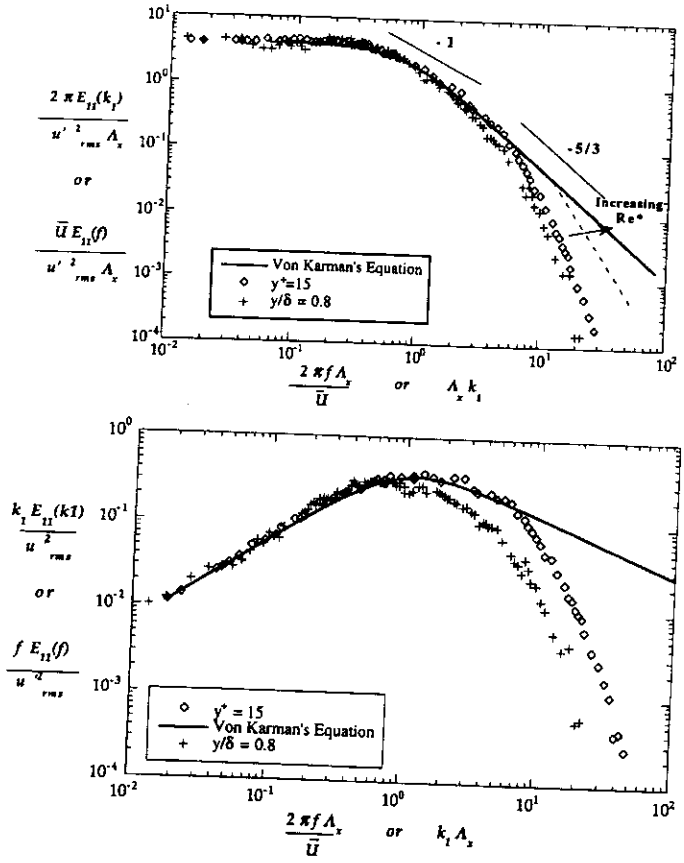

FIGURE 13.22 Power spectral densities for wall bounded turbulent flows (sample data from a boundary layer with $Re^* = 320$). (a) Normalized power spectral density, (b) energy content at a given wave number.

Hence normalizing $E_{11}(k_1)$ with $u'^2_{rms}\Lambda_x$, as in Fig. 13.22a, forces a collapse of the data as k_1 approaches zero. The $E_{11}(k_1)$ spectra for positions from the outer part of a boundary layer to very close to the wall ($y^+ = 15$) follow the Von Kármán equation well for low wavenumbers, i.e., the larger scale turbulent eddies. At higher wavenumber, $E_{11}(k_1)$ falls below the Von Kármán equation prediction — this is due to viscous dissipation of the turbulent eddies which becomes significant at higher wavenumbers. As indicated on Fig. 13.22a, the fall-off from the Von Kármán equation due to viscous dissipation occurs at higher k_1 for increasing Reynolds number.

Three different regimes in the wavenumber domain are believed to exist for the scaling of the power spectal density for turbulent wall flows. The low wavenumber regime has been found to scale with the outer variable δ — note this is consistent with the collapse of the spectral data shown in Fig. 13.22a since Λ_x is proportional to δ. The intermediate wavenumber range scales with distance from the wall, y, which is considered an inner variable. The large wavenumber range scales with the Kolmogorov length scale, which is consistent with viscous dissipation being dominant for the higher wavenumbers. Note that an important implication of these three different scaling regimes in the wavenumber domain is that different scaling of turbulence occurs not only at different distances from the wall, but at different wavenumbers at any given position. Furthermore, the spectra show that outer scaled effects occur even in the near wall region, and wall and viscous effects are noticeable even far from the wall.

Also indicated on Fig. 13.22a are regions of k_1^{-1} and of $k_1^{-5/3}$ decay for the power spectral density. The region of $k_1^{-5/3}$ decay, often called the inertial subrange, is predicted for isotropic turbulence small enough

to be independent of large scale motions, yet large enough so that energy is transferred from larger scale eddies to smaller scale eddies with negligible viscous dissipation. The k_1^{-1} region is predicted from the overlap of the outer δ scaling of the largest eddies and the inner y scaling.

The relative energy levels of eddies with different wavenumbers (sizes) is more readily apparent from the $k_1 \cdot E_{11}(k_1)$ product. Figure 13.22b shows the power spectra in this form where it is apparent that the most energetic eddies occur at a wavenumber of $k_1 \approx 1/\Lambda_x$, i.e., eddies of the size of the integral length scale. Also evident from Fig. 13.22b is that there are significant energy levels over a very broad range of wavenumbers of about a two decade range. This range of wavenumbers with significant energy levels increases with increasing Reynolds number.

Noncanonical Flows: Surface Roughness, Pressure Gradients, and High Free-Stream Turbulence

Surface Roughness

Surface roughness causes large increases in surface drag and substantially alters the turbulence characteristics near the wall. A surface is considered aerodynamically smooth (roughness has no noticeable effects) if the heights of the roughness elements are less than $k_s^+ = 5$, where k_s is the sandgrain size for uniformly distributed sandgrain roughness. For many practical flows this is actually quite small, so that roughness effects are a common occurrence.

With roughness elements protruding into the flow, pressure forces on these elements can be a dominant component of the drag force on the surface. When pressure forces dominate, the flow is said to be fully rough and viscous effects are negligible. Fully rough flow typically occurs for $k_s^+ > 70$, and the intermediate regime where both viscous and pressure effects are important, $5 < k_s^+ < 70$, is known as transitionally rough. Although these limits are given in terms of sandgrain roughness height (as are many correlations), equivalent sandgrain roughness heights can be determined for other types of rough surfaces [22]. Most rough surfaces are categorized as "k type" in which the roughness effects on the flow scale with roughness height k. The other category of roughness is known as "d type" for which the roughness elements are large and closely spaced so that the flow passes over the top of the elements with stagnate fluid between the elements. Velocity field characteristics for d type roughness scale with the boundary layer thickness or width of the internal flow geometry.

The correlation for the friction factor f for pipe flows presented in Table 13.1 includes the roughness parameter ε/D where ε is the roughness height and D is the pipe diameter. Roughness heights as small as $\varepsilon/D = 10^{-3}$ will cause significant increases in the friction factor and hence pressure losses. For a flat plate, if the roughness is known to be large enough such that fully rough flow occurs, the correlation for skin friction coefficient C_f presented in Table 13.1 is applicable. Note that for rough walls this "skin friction" is actually primarily pressure forces on the roughness elements.

Using inner scaling, the mean velocity profiles for rough surface flows follow the same logarithmic profile as for smooth surfaces, except that there is a $-\Delta u^+$ displacement of the profile, i.e.,

$$u^+ = \frac{1}{\kappa} \ln\left(y^+\right) + C - \Delta u^+ \tag{13.59}$$

The $-\Delta u^+$ displacement increases with increasing roughness. For fully rough flows viscous effects are negligible, and scaling with respect to y^+ is not appropriate. The appropriate length scale is k_s and the near wall mean velocity profile becomes

$$u^+ = \frac{1}{\kappa} \ln\left(\frac{y}{k_s}\right) + 8.5 \tag{13.60}$$

The outer region of the mean velocity profile is unaffected by surface roughness. Somewhat surprisingly the u'_{rms} turbulence levels in the near wall region decrease when scaled with u_τ (but turbulence intensity,

$u'_{rms}/\overline{U}$, does increase). In the outer region, there is no affect of roughness on u'_{rms}/u_τ when scaled with y/Δ. The Reynolds shear stress is unaffected by roughness from the peak of the $\overline{u'v'}$ level near the wall through the outer region [18].

Streamwise Pressure Gradients

Streamwise pressure gradients can cause significant changes in an external turbulent wall flow. Positive (adverse) streamwise pressure gradients can greatly increase turbulence levels, but decreases wall shear, and eventually causes separation from the wall. Negative (favorable) pressure gradients suppress turbulence, but cause increases in wall shear. Tubulence levels can be suppressed to such an extent by negative pressure gradients that relaminarization occurs. Relaminarization occurs for pressure gradients greater than $K = 3 \times 10^{-6}$ where K is defined as

$$K = \frac{\nu}{\overline{U}^2}\frac{d\overline{U}}{dx} \tag{13.61}$$

K is a useful parameter for characterizing the strength of the pressure gradient since it is independent of the state of the boundary layer. In general, turbulent boundary layers subjected to streamwise pressure gradients will not be in equilibrium, i.e., have similarity velocity profiles in the outer part of the boundary layer that are invariant with streamwise distance. However, for some specific pressure distributions, equilibrium flows do occur. In particular, equilibrium turbulent boundary layer flows will occur when the Clauser parameter for pressure gradients, β, is constant along the length of the surface. The Clauser parameter is defined as

$$\beta = \frac{\delta^*}{\tau_w}\frac{d\overline{P}}{dx} \tag{13.62}$$

The Clauser parameter will be constant for flows in which the free-stream velocity varies as $\overline{U}_\infty \sim x^m$ or $\overline{U}_\infty \sim \exp x$ and $d\Delta/dx$ is constant. Note that β can be interpreted as the ratio of pressure forces on the boundary layer to the wall shear forces. Consequently values of β greater in magnitude than 1 indicate strong pressure effects.

Because the pressure gradient effect on the mean velocity is nonlinear, a favorable pressure gradient causes a fuller velocity profile for a boundary layer, i.e., the boundary layer profile is more uniform. Consequently, for the same boundary layer thickness, there is an increased velocity gradient at the wall resulting in increased wall shear. Similarly, adverse pressure gradients cause a decrease in wall shear. Representative mean velocity profiles for equilibrium streamwise pressure gradient flows are given in Fig. 13.23 [17]. The inner layer of the velocity profile is not affected by either favorable or adverse pressure gradients. The "fuller" velocity profile discussed above results in diminished wake strength for favorable pressure gradients, whereas the reduced fullness of the profiles for adverse pressure gradients results in increased wake strengths. A correlation for the wake strength of equilibrium flows as a function of β (suggested by White [25]) is

$$\Pi \approx 0.8\,(\beta + 0.5)^{0.75} \tag{13.63}$$

The increase or decrease of turbulence levels due to imposed streamwise pressure gradients can be attributed to production of turbulence energy by the streamwise velocity gradient. Referring to the turbulent kinetic energy equation, Eq. (13.8) in Section 13.1, shows the production of turbulence is proportional to $-\overline{u'u'}(\partial\overline{U}/\partial x)$, indicating a decrease in turbulence for accelerating flows (favorable pressure gradients), and an increase in turbulence for decelerating flows (adverse pressure gradients). Examples of turbulence statistics for equilibrium turbulent boundary layers subject to adverse pressure gradients are shown in Fig. 13.24 [17]. The u'_{rms}, v'_{rms}, and $\overline{u'v'}$ statistics are relatively unaffected in the inner region, $y^+ < 50$, but increase substantially in the outer region. The increase in Reynolds shear stress $\overline{u'v'}$ due to adverse pressure gradients is also predictable from a momentum balance analysis, Eq. (13.45), in which it is evident that near the wall the forces due to pressure gradients will be balanced by increases in Reynolds shear stresses.

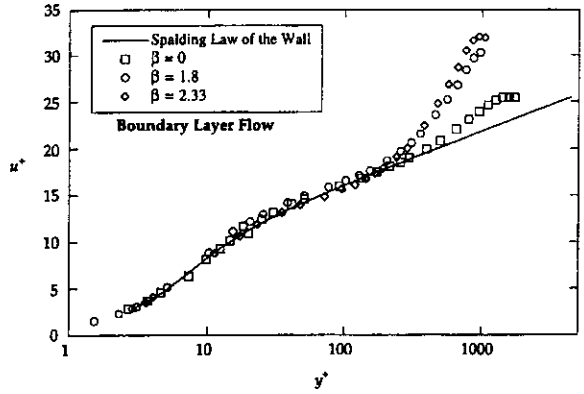

FIGURE 13.23 Pressure gradient effects on the mean velocity profile of a boundary layer flow. (*Source:* Koske, J. E. and Tiederman, W. G., Report PME-FM-91-3, Purdue University, 1991.)

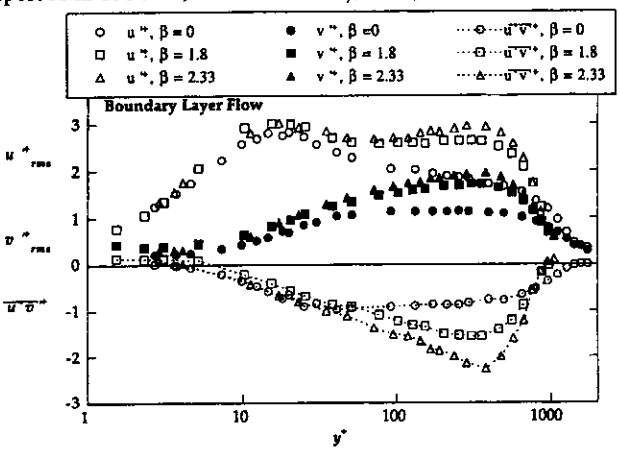

FIGURE 13.24 Pressure gradient effects on the rms velocities and Reynolds shear stress profiles of a boundary layer flow. (*Source:* Koske, J. E. and Tiederman, W. G., Report PME-FM-91-3, Purdue University, 1991.)

Free-Stream Turbulence

High levels of free-stream turbulence affect turbulent boundary layers causing increases in skin friction and altering the velocity statistics in the outer part of the boundary layer. The effects of free-stream turbulence are dependent not only on the turbulence level, typically quantified by $Tu = u'_{rms}/\overline{U}$, but also on the length scale of the free-stream turbulent eddies, quantified through either the integral length scale (Λ_x) or dissipation length scale (L_u^ε) where the dissipation length scale is given by the following relation:

$$L_u^\varepsilon \equiv -\frac{\left(u'^2_{rms}\right)^{3/2}}{\overline{U}_\infty \frac{d\left(u'^2_{rms}\right)}{dx}} \tag{13.64}$$

Increases in skin friction due to high free-stream turbulence levels are quantified in Fig. 13.25 in terms of the ratio $(C_f - C_{f,o})/C_{f,o}$ where $C_{f,o'}$ is the skin friction coefficient with zero free-stream turbulence at the same Re_θ. Note that the data in Fig. 13.25 are correlated using the HB parameter [11], which is based on a combination of turbulence level and dissipation length scale. The HB parameter is as follows:

$$HB = \frac{Tu(\%)}{\left(\frac{L_u^\varepsilon}{\delta_{99}} + 2\right)} \tag{13.65}$$

The effect that free-stream turbulence has on the boundary layer is primarily in the outer region. As free-stream turbulence levels increase, the wake strength for the mean velocity profile decreases, and the wake strength actually becomes negative for very high free-stream turbulence levels. Elevated turbulence intensities are found throughout the outer region, but the turbulence levels near the wall are unaffected except for very high free-stream turbulence levels of $Tu > 12\%$.

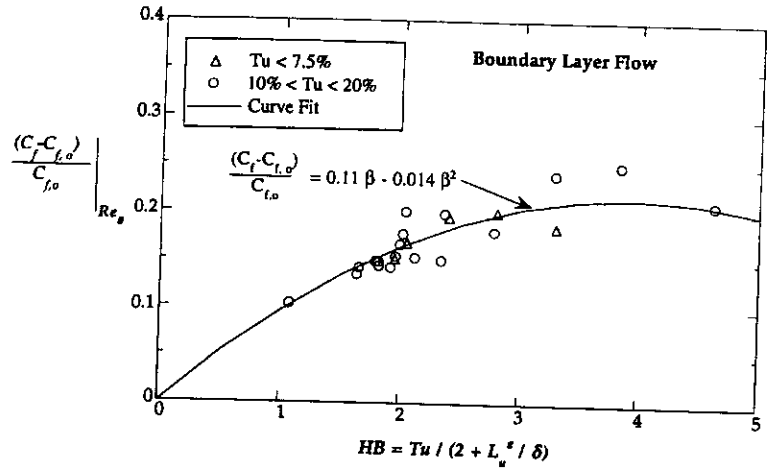

FIGURE 13.25 Increases in the coefficient of friction C_f for turbulent boundary layer flows subjected to high free-stream turbulence levels Tu with dissipation length scales $L_u{}^\varepsilon$. (*Source:* Johnson and Johnston [15], Ames and Moffat [1], and Thole and Bogard [24].)

References

[1] Ames, F. E. and Moffat, R. J., Heat transfer with high intensity large scale turbulence: The flat plate turbulent boundary layer and the cylindrical stagnation point, Stanford Univ. Report HMT-44, 1990.

[2] Browne, L. W. B. and Antonia, R. A., The frequency response of cold wires. *Proceedings of the Seventh Symposium on Turbulence,* Rolla, Missouri, 1988.

[3] Bruns, J., Dengel, P., and Fernholz, H.H., Mean flow and turbulence measurements in an incompressible two-dimensional turbulent boundary layer. Part I; Data. Institutsbericht Nr. 02/92, Hermann-Föttinger-Institut für Thermo- and Fluiddynamik Technische Universität Berlin, 1992.

[4] Clauser, F. H., Turbulent boundary layers in adverse pressure gradients, *J. Aerospace Sci.,* 21, 91, 1954.

[5] Clauser, F. H., The turbulent boundary layer, in *Advances in Applied Mechanics,* Vol. 4, Academic Press, New York, 1956.

[6] Colebrook, C. F., Turbulent flow in pipes with particular reference to the transition between the smooth and rough pipe laws, *J. Inst. Civ. Eng. London,* 11, 1989.

[7] Coles, D., The turbulent boundary layer in a compresible fluid. The Rand Corporation, Re. R-403-PR, 1962.

[8] Dean, R. B., Reynolds number dependence of skin friction and other bulk flow variables in two-dimensional rectangular duct flow, *ASME J. Fluids Eng.,* 100, 215–223, 1978.

[9] Edwards, R. V., Report on the special panel on statistical particle bias in laser anemometry, *ASME J. Fluids Eng.*, 109, 89–93, 1987.
[10] Gerhart, P. M., Gross, R. J., and Hochstein, J. I., *Fundamentals of Fluid Mechanics*, 2nd ed., Addison-Wesley, New York, 1992.
[11] Hancock, P. E. and Bradshaw, P., The effect of free-stream turbulence on turbulent boundary layers, *ASME J. Fluids Eng.*, 105, 284, 1983.
[12] Harder, K. J. and Tiederman, W. G., Influence of wall strain rate, polymer concentration and channel height upon drag reduction and turbulent structure, Technical Report PME-FM-89-1, Purdue University, 1989.
[13] Hinze, J. O., *Turbulence*, 2nd ed., McGraw-Hill, New York, 1975.
[14] Johansson, A. V. and Alfredsson, P. H., Effects of imperfect spatial resolution on measurements of wall bounded turbulent shear flows, *J. Fluid Mech.*, 137, 409, 1983.
[15] Johnson, P. L. and Johnston, J. P., Active and inactive motions in a turbulent boundary Layer—Interactions with free-stream turbulence, 7th Symposium on Turb. Shear Flows, 20.2.1-6, 1989.
[16] Kays, W. M. and Crawford, M. E., *Convective Heat and Mass Transfer*, 3rd ed., McGraw-Hill, New York, 1983.
[17] Koske, J. E. and Tiederman, W. G., Turbulence structure and polymer drag reduction in adverse pressure gradient boundary layers, Report PME-FM-91-3, Purdue University, 1991.
[18] Ligrani, P. M., Structure of turbulent boundary layers. Aerodynamics and compressible flows, *Encyclopedia of Fluid Mechanics*, Cheremisinoff, N., Ed., Vol. 8, 111–189, Gulf Publishing, 1988.
[19] Nakayama, A. and Westphal, R. V., Effect of sensor length and spacing on X-wire measurements in a boundary layer, NASA TM-88352, 1986.
[20] Nikuradse, J., Similarity for turbulent flow in smooth pipes. VDI-Forschungsh., No. 356, English translation NACA TT F-10: 359, 1932.
[21] Schlichting, H., *Boundary Layer Theory*, 6th ed., McGraw-Hill, New York, 1968.
[22] Sigel, A. and Danberg, J. E., New correlation of roughness density effects on the turbulent boundary layer, *AIAA J.*, 28, 554–556, 1990.
[23] Spalding, D. B., A single formula for the law of the wall, *ASME, J. Appl. Mech.*, 28(3), 1961.
[24] Thole, K. A. and Bogard, D. G., Enhanced heat transfer and skin friction due to high free-stream turbulence, *ASME J. Turbomachinery*, 117(5), 418–424, 1994.
[25] White, F. M., *Viscous Fluid Flow*, 1st ed., McGraw-Hill, New York, 1974.
[26] White, F. M. *Fluid Mechanics*, 3rd ed., McGraw-Hill, New York, 1994.